Further Remarks on Stochastic Damage Evolution of Brittle Solids under Dynamic Tensile Loading

S. Mastilovic*

Faculty of Construction Management, Union University,
Cara Dusana 62-64, 11000 Belgrade, Serbia

ABSTRACT: This paper illuminates some general features and provides elementary interpretations of the deformation, damage, and failure of brittle solids characterized by very low fracture energy. The dynamic response of these materials is determined to a large extent by stochastic and random factors. The investigation emphasis is on the moderate-to-extremely high rate range [10 s^{-1}, 1×10^{9} s^{-1}], explored under practically identical in-plane stress conditions. The statistical approach is based on repeated particle dynamics simulations for different physical realizations of micromechanical disorder of a two-dimensional (2D) brittle discrete system. The proposed strategy is computationally intensive, which necessitates simplicity of the laws governing the interparticular interaction. Based on the simulation results, an expression is proposed to model the mean tensile strength dependence on the strain rate. The linearity of the rate dependence of the stress-peak macroscopic response parameters is observed and discussed.

KEY WORDS: brittle systems, dynamic strength, damage energy rate, time to failure, disorder

INTRODUCTION

Brittle materials (ceramics, rocks, concrete) are often used in civilian and military applications for design of structural components exposed to extreme dynamic loads. These applications require a thorough knowledge of the physics of high-rate deformation of said materials, which is complex and subtle and influenced substantially by stochastic and random factors. In addition to being nonstationary, the considered phenomena are nonlinear and far from equilibrium, which often makes them too recondite to be modeled theoretically. Besides, although damage evolution by its very nature spans spatial scales, the recent simulation results (Mastilovic et al., 2008) suggest that the governing spatial scale of damage and rupture phenomena in the low-fracture energy materials changes with the loading rate: the high-rate damage is governed by events at the submicroscopic scales while the medium-rate damage is governed substantially, if not predominantly, by cooperative phenomena at the mesoscopic scale ("the disorder of micro-texture controls the macroresponse"; Rinaldi, 2009). Last but not least, the complexity of analytical and computational modeling is emphasized by a dearth of detailed test data, especially with respect to direct measurements under the high-rate tensile loading.

The present empirical investigation is the last part of a trilogy (Mastilovic et al., 2008; Mastilovic, 2010) pertaining to analysis of stochastic damage evolution of the dynamically loaded brittle systems. An objective of this study is to provide further insights into some salient features of the deformation dynamics of brittle solids, specifically the ceramic materials with the inferior grain boundary strength and low fracture energy. With these materials in mind, the strain rate range of these virtual idealized experiments [10 s^{-1}, 1×10^{9} s^{-1}]—tentatively labeled medium-to-high—reaches the theoretical limit,

* Tel.: +381 11 218-0287, e-mail: gmvv@eunet.rs

$\dot{\varepsilon}_0 = \varepsilon_0/\tau_0 \approx 10^9\ s^{-1}$; defined by the assumed limit failure strain, ε_0=0.001, and a temporal parameter of the order of Debye's atomic vibration period, $\tau_0 = 10^{-12}\ s$ (Qi et al., 2009). The lower and upper ends of the range investigated herein are customarily explored by the split Hopkinson bar (below $10^4\ s^{-1}$) and the planar impact tests (up to $10^8\ s^{-1}$), respectively (Field et al., 2004). The former is performed under one-dimensional stress conditions while the latter is performed under one-dimensional strain conditions, which renders the direct comparison of results somewhat tentative (Grady, 1995).

The lattice simulations, in spite of well documented particularities and limitations (Hansen et al., 1989; Jagota and Bennison, 1994; Monette and Anderson, 1994; Ostoja-Starzewski, 2002; Van Mier and Man, 2009), replicate rather well the most prominent aspects of the sample response including the essential features of rate-dependent fracture (microcracking, damage localization, fragmentation, comminution) and deterioration of the effective stiffness, and provide an elementary intuition on the phenomena (Mastilovic and Krajcinovic, 1999). Additionally, they prove a useful tool for qualitative analysis of universal trends of the dynamic behavior of brittle materials for a number of reasons. First, they enable the extrapolation of experimental results into the regions that are still beyond capabilities of the presently available experimental techniques. Second, the virtually unlimited control over computational experiments offers detailed insights in the deformation process. Moreover, an often-advertised advantage of the discrete system methods in the statistical damage mechanics is that they incorporate both aleatory variability and epistemic uncertainty in a straightforward manner. The natural randomness of the mesoscale material texture is an example of the aleatory variability. The intrinsic (pre-existing) disorder is, in the course of deformation, further enhanced by the extrinsic disorder due to the damage evolution that is governed (to an extent depending on deformation rate; Mastilovic et al., 2008) by the local fluctuations of energy barriers quenched within the material and the local fluctuations of stress. The nonlocal and nonlinear character of these far-from-equilibrium processes is such that concepts of strain and damage (and temperature, in general) based on spatial and temporal averaging are, at best, conditionally acceptable (Mastilovic and Krajcinovic, 1999). Nevertheless, the overall quantities exhibit universal trends (Hansen et al., 1989) despite the random character of the local fluctuations of mechanical fields. The particle-based methods (e.g., Cundall and Strack, 1979; Jirasek and Bazant, 1995; Mastilovic and Krajcinovic, 1999; Liu et al., 2008) require a relatively modest computational effort allowing for consideration of a representative sample of physical realizations of a given statistics. This property of particle dynamics is crucial for the extraction of universal trends from the data rendered irregular by the randomness of the brittle system.

SIMULATION MODEL

The present simulation model was used extensively in the past decade and described fairly well in literature (e.g., Mastilovic and Krajcinovic, 1999), thus, only a brief summary is deemed necessary herein. The brittle continuum is approximated by a virtual 2D structure (a hexagonal particle network) that is, in absence of micromechanical disorder, equivalent to the three-dimensional elastic continuum under the plane strain conditions (Monette and Anderson, 1994).[1] The discrete system is formed by "continuum particles" of mass m (Wiener, 2002) that interact through brittle nonlinear bonds. In the present mesoscale model, each particle represents a grain of polycrystalline alumina (Al_2O_3); consequently, the particle network "does not convey explicit information about geometry but about mechanical properties and the topology of the microscale of the material" (Rinaldi et al., 2008). Since the microstructural morphology of the ceramic material is not perfect, the discrete system is necessarily disordered.

The system of interconnected particles is a simplical topologically-ordered Delaunay network dual to the Voronoi froth of the ceramic grain boundaries (Curtin and Scher, 1990) that are related by a Legendre transformation (Zallen, 1983).

[1] As soon as the randomness is introduced, the behavior of a material could only be approximated by the behavior of the 2D lattice, with the degree of accuracy that decreases with the level of disorder "quenched" within the system (Mastilovic, 2008).

The geometrical disorder is introduced by the normal distribution of stress-free interparticular distances λ_0 within the range $\left[\alpha\,\bar{\lambda} \le \lambda_0 \le (2-\alpha)\bar{\lambda}\right]$. The geometrical-order parameter α, ($0 < \alpha \le 1$), is the model property that defines bandwidth of the material's geometrical disorder (i.e., it is a measure of grain size and shape versatility). The average interparticular distance, $\bar{\lambda}$, defines the model resolution length, l_c. All finer-scale intrinsic defects ("Griffith flaws": submicroscopic flaws, glassy pockets, microcracks or other centers of heterogeneity; Lawn, 1993) have to be taken into account by the stiffness and/or failure strain distributions of interparticular bonds.

The structural disorder, introduced through a distribution of the interparticular bond stiffnesses, is related to the effect of randomly distributed residual stresses (Curtin and Scher, 1990; Raiser et al, 1990; Krajcinovic, 1996), and various finer-scale defects and heterogeneities ("transitory obstacles", Lawn, 1993) that tend to accumulate at grain boundaries of ceramics, which makes these lower-density regions structurally inferior in comparison with the bulk material and, consequently, "the most common examples of weak interfaces in brittle materials" (Lawn, 1993). The stiffness distribution of interparticular bonds is assumed to be uniform within $\left[\beta\,\bar{k} \le k \le (2-\beta)\bar{k}\right]$, where β ($0 \le \beta \le 1$) is the structural-order parameter. The mean stiffness of interparticular bonds comprising the discrete network is related to the modulus of elasticity of the pristine material, $\bar{k} = 8\sqrt{3}\,E_0/15$, which provides an important connection between mechanical properties of the material and the discrete 2D system. It cannot be overemphasized that this stiffness distribution encompasses effects, on damage dynamics, of all structural features smaller than the resolution length. Consequently, since the resolution length is equal to the grain facet, the activation/nucleation and growth of all finer-scale defects (e.g., Kuksenko et al., 1975) from their initial length to the length of the grain boundary facet is necessarily instantaneous.

It is noteworthy that the only dissipative mechanism in the present model, developed specifically for the highly brittle materials, is the bond rupture corresponding to the intergranular microcrack nucleation. The bond between mass particles i and j (dual to the corresponding grain boundary facet) ruptures when its elongation reaches the critical value $\varepsilon_{cr} = \Delta\lambda_{ij}/\lambda_{0ij} = 0.1\%$, which is the model parameter that can be determined from the uniaxial strength of the material.

In hindsight, $\varepsilon_{cr} = 0.1\%$ proves to be somewhat too small in conjunction with $\alpha = 0.2$, $\beta = 0.9$ and free lateral boundaries, since it leads to an underestimate of the quasi-static failure strain of the sample. The selected value of α ensures, within topological limitations of the model, reasonable resemblance between the particle network and the typical grain structures of ceramics (e.g., Lawn, 1993; Sarva and Nemat-Nasser, 2001; Espinosa and Zavattieri, 2003). The relatively high value of β is, in absence of experimental data guidance, adopted from the preceding disorder-effect study (Mastilovic, 2010). The procedures for creating a mechanically equivalent lattice capable of matching the physical properties of engineering ceramics and, consequently, *quantitative* estimates of their mechanical response are proposed by Rinaldi et al. (2008) with emphasis, among others, on rigorous Voronoi tessellation and "calibration" of the major statistics of the given microstructure.

COMPUTER SIMULATIONS OF UNIAXIAL TENSION

The tensile specimen is a ceramic square with L=1.9 *mm*, modeled by a 192×227 lattice. The mesh objectivity of results obtained by using this lattice size is originally investigated by Mastilovic and Krajcinovic (1999); an additional illustration of its representativeness is also added in this paper.[2]

The problems of the uniform distribution of load within the sample and loading at the extremely high rates are solved by imposing an initial velocity field on all mass particles:

$$\dot{x}_1\left(t=0\right) = \dot{\varepsilon}_1\, x_1 \tag{1a}$$

[2] The rupture and size effects of the quasi-statically loaded brittle central-force lattices were analyzed by Hansen et al. (1989) who suggested various scaling relations of physical parameters and a multifractal distribution of lattice forces in the softening phase of deformation.

$$\dot{x}_2(t=0) = -\upsilon_0^{(\varepsilon)}\,\dot{\varepsilon}_1\,x_2 \tag{1b}$$

defined in terms of the prescribed strain rate, $\dot{\varepsilon}_1 = \dot{L}/L$, and the plane-strain Poisson's ratio, $\upsilon_0^{(\varepsilon)}$. Holian and Grady (1988) used a similar approach to model the adiabatic expansion.

Subsequently, at $t > 0$, only velocity of the particles located at the specimen longitudinal boundaries ($x_1 = \pm L/2$) is controlled $\dot{x}_1 = \pm\,\dot{\varepsilon}_1\,L/2$, while the motion of all other particles is governed by the Newton's equation of motion. The lateral specimen boundaries ($x_2 = \pm L/2$) are free.

The effects of this loading procedure are demonstrated in literature (as reported by Mastilovic et al., 2008).

The parameters recorded continuously throughout the entire simulation—the position and velocity of each particle ($\vec{x}, \dot{\vec{x}}$) and the number of ruptured links (n)—suffice to compute the volume averaged stress and stiffness components, scalar damage, and potential, kinetic and damage (released cohesive) energies of the discrete system.

Specifically, the damage energy released by rupture of n links (of stiffness k and initial length λ_0) is

$$\mathrm{E}_D = \frac{1}{2}\sum_{1}^{n} k\lambda_0^2\varepsilon_{ci}^2 \tag{2a}$$

while the components of the stress tensor are

$$(\sigma_i)_{\alpha\beta} = \frac{1}{2\Omega}\sum_{\substack{i,\,j \\ j\neq i}} \frac{d\phi}{d\lambda_{ij}}\frac{(\lambda_{ij})_\alpha\,(\lambda_{ij})_\beta}{|\lambda_{ij}|} \tag{2b}$$

In Equation (2b), Ω is the sample volume, while $(\lambda_{ij})_\alpha$ and $(\lambda_{ij})_\beta$ are the α and β components of the distance vector λ_{ij} between particles i and j. This expression is simplified approximating the particle interaction by the central force pair-potential $\phi = \hat{\phi}(\lambda_{ij})$.

SIMULATION RESULTS

Damage Patterns and Stochastic Effects on Damage Growth

The characteristic damage patterns are unambiguous signatures of the loading rate, which result from the complex fracture physics on the microscopic and mesoscopic scales driven by interplay of the strain rate and the material disorder. The rate-dependent evolution and pattern of damage accumulation are closely related to the shape of stress-strain curve and the damage energetics (Mastilovic et al., 2008; Mastilovic, 2010).

The dynamic response of the low fracture energy materials subjected to the extremely high loading rate ($\dot{\varepsilon} \geq 1\cdot 10^6\ s^{-1}$, Region 3 in Figure 4) is characterized by:

(i) microscale uniformity (i.e., uniform distribution of microcracks),
(ii) damage evolution that is not correlated,
(iii) negligible damage accumulation in the hardening phase of uniaxial tensile deformation,
(iv) minimum fragment size, and
(v) negligible stochasticity that reflects diminishing influence of the material disorder (Figure 1a).

It has been argued (Grady, 1995; Zhou and Molinari, 2004; Qi et al., 2009) that, at these rates, the delay due to damage kinetics inhibits the propagation and coalescence of activated microcracks; which, consequently, leads to activation or nucleation of other microcracks before the adjacent already-activated microcracks have time to extend and unload them.

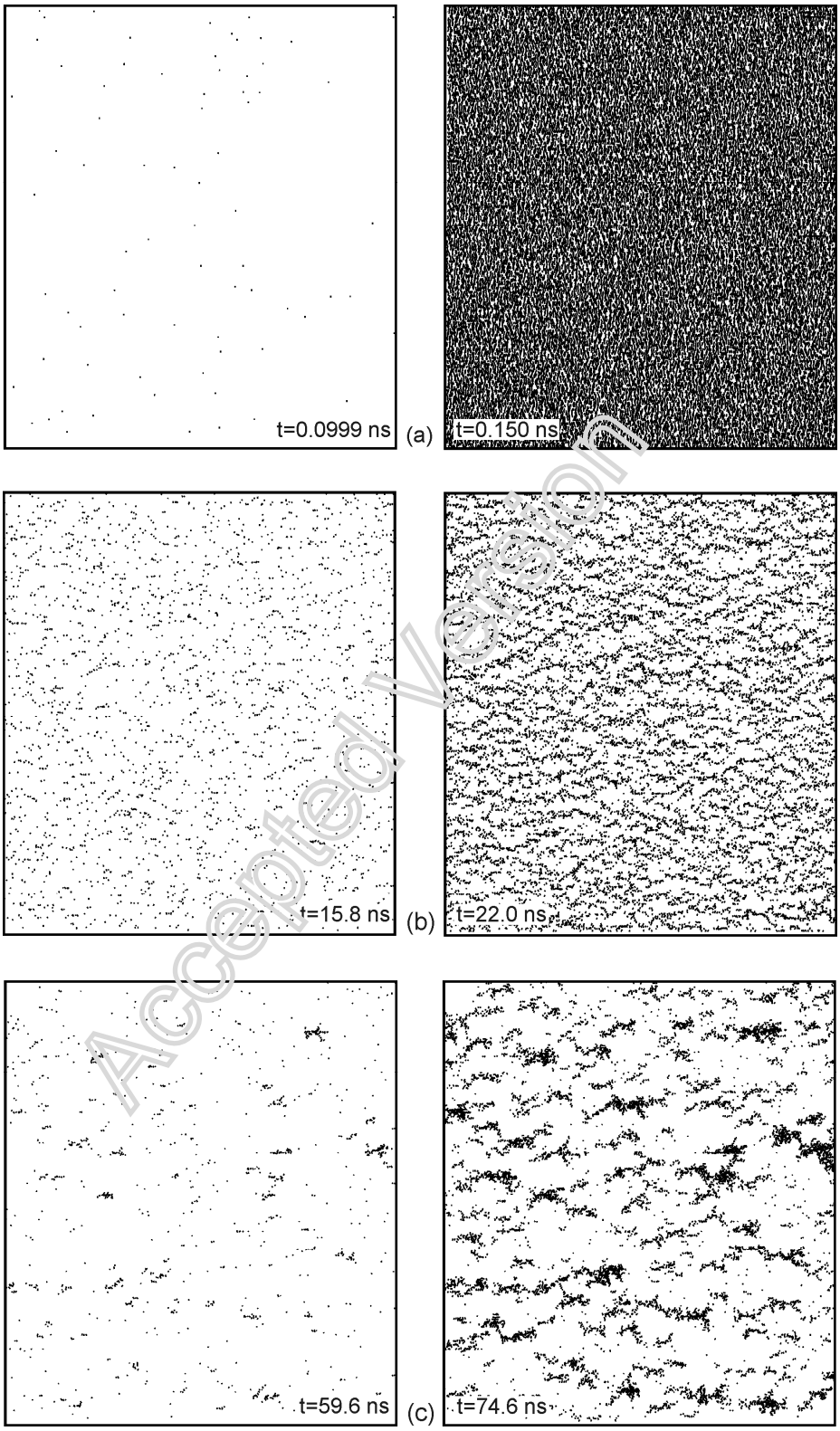

Figure 1. *Typical damage patterns at three different loading rates: (a) 1×10^{7} s^{-1}, (b) 5×10^{4} s^{-1}, (c) 1×10^{4} s^{-1}. The snapshots on the left side correspond to the damage pattern at the peak of each stress-strain curve, marking the onset of localization. (Dashes represent broken links.)*

The left snapshot in Figure 1a, corresponding to a damage pattern at the peak of the stress-strain curve, reveals negligible uniformly-distributed uncorrelated[3] damage growth in the hardening phase, followed by an avalanche of micro-failures at the softening phase threshold. Eventually, the overwhelming majority of favorably oriented links is broken (Figure 1a), which is reflected by a very high damage density.

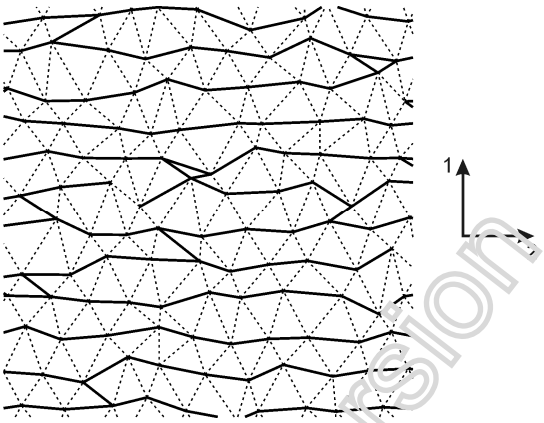

Figure 2. *Typical anisotropic damage pattern by the end of softening phase for $1\times10^7\ s^{-1}$. (The solid and dashed lines represent the remaining and broken links, respectively.)*

Eventually, by the end of the softening phase (t_F), $\lim_{t\to t_F} D = \lim_{t\to t_F}(n/N) \approx 2/3$, which results not only in complete loss of load-carrying capacity in the loading direction but also in failure of practically every link that is not predominantly perpendicular to the loading direction (Figure 2). Effectively, in this stage, the independent micro-failure events have developed to such extent that the material becomes "structuralized" (Wang and Ramesh, 2004), if not comminuted, due to "damage percolation" in the lateral direction (Figure 2). The strongly anisotropic damage structure resembles the one-grain wide columns produced by the splitting under far-field uniaxial compression that were analyzed by Bhattacharya et al. (1998). The related "spectral form" of damage distribution was discussed in detail by Rinaldi (2009) for the statically loaded lattice.

An increasing influence of the microstructural heterogeneity (the original and load-induced one) on the macroscopic material response results in a complex damage evolution "involving nucleation and propagation of myriad microcracks that finally coalesce" (Drugan, 2001), (Figures 1b and 1c). Thus, the dynamic response of highly brittle materials subjected to the high loading rate (tentatively, $1\times10^4\ s^{-1} < \dot{\varepsilon} < 1\times10^6\ s^{-1}$, Region 2 in Figure 4) is characterized by:

(i) mesoscale uniformity (i.e., uniform distribution of microcrack clusters),
(ii) damage growth driven by cooperative phenomena,
(iii) significant damage accumulation in the hardening phase of deformation,
(iv) mesoscale fragment size defined by the network of microcrack clusters, and
(v) increased stochasticity that reflects increase of influence of the material disorder.

At these transitional rates the interplay between athermal fracture and damage kinetics governs the brittle response (Qi et al., 2009), which leads to the surge of strength with the strain rate increase (Region 1 → Region 2, Figure 4). This rate-driven transition is reminiscent of brittle-ductile transition (Grady, 1995). The microcrack clusters, which dominate the damage patterns at the softening-phase end

[3] The use of the term "uncorrelated" merits a clarification: in the present context it implies independent microcrack nucleation or activation events (that take place in absence of significant cooperative phenomena).

of the $\dot{\varepsilon}_1 = 1\times10^4\ s^{-1}$ simulation (Figure 1c), comprise a plethora of broken bonds. These microcrack clouds constitute a link between the elementary micro-fracture event and the dynamic macro-failure phenomenology. They are, also, an example of the effect that external actions can have on the internal structure of material reflected by formation of a new structure by the localization process. Mishnaevsky (1998) suggested that the damage localization into the high- and low-damage regions is analogous to the formation of dissipative structures in nonlinear systems with stochastic effects. The cooperative phenomena on both microscopic and mesoscopic scale (signaled by the growth of clusters and their interactions) play an essential role in the fracture process and the final sample-destruction mode. This is reflected by notably nonlinear character of the hardening phase and the pronounced softening phase of the stress-strain curve (Mastilovic et al., 2008).

It is interesting to note that, fortuitously or not, the typical vertical distance between dominant clusters, D_{cl}, for the transitional rates (Region 2, Figure 4) suggested by snapshots, such as those on right side on Figure 1b and 1c, agree well with the fragment size prediction, $l_f \propto \dot{\varepsilon}^{-2/3}$, based on the Drugan's (2001) model as indicated by Figure 3, which deserves explanation not available at present. The same model also predicts that the minimum possible fragment size for the present mesoscale computational model (equal to the resolution length, $l_c \approx 10\ \mu m$) would be achieved at $\dot{\varepsilon} \approx 1\times10^7\ s^{-1}$, which corresponds to the theoretical strength approach in Figure 4.

With further decrease of the loading rate, the dynamic response is distinguished by the localization of microcracks in only a couple of clusters; in the limit case of quasi-static loading, often into a single dominant cluster (Mastilovic and Krajcinovic, 1999).[4] The quasi-static tensile strength (σ_{m0}) is, thus, defined by the critical weak link (microscopic-scale flaw or defect) and thermally-activated subcritical growth of a crack (of length a) governed by Griffith's formulation: $G(t,a) \le G_c$, $\left[G(t,a) - G_c\right]\dot{a} = 0,\ t \ge 0$. The failure strain is significantly smaller than the critical micro-strain (Mastilovic et al., 2008).

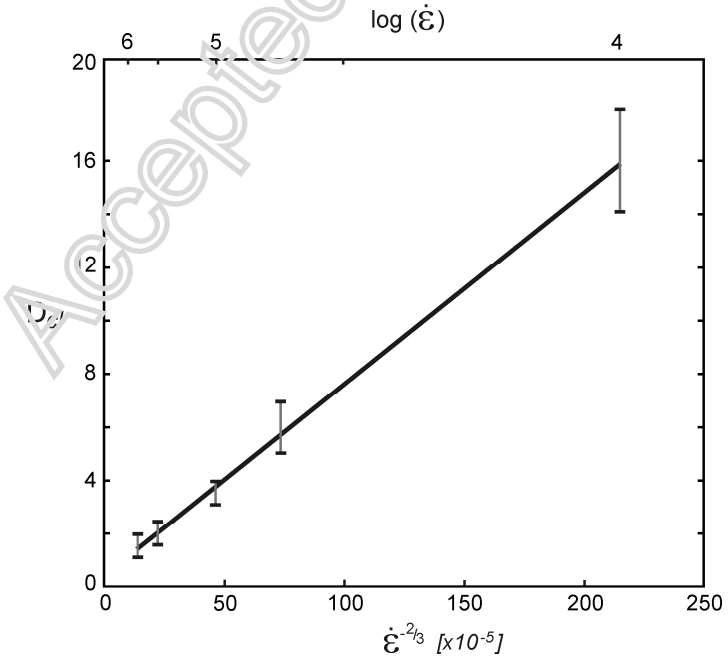

[4] Simulations of the low-rate deformation by the dynamic technique were not performed in this analysis since they require substantial increase in computational effort (e.g., Liu et al., 2008), which virtually precludes statistical analyses of the kind presented herein.

Figure 3. *Strain rate dependence of typical distance in the loading direction between dominant clusters at the end of softening in the transitional range (Region 2 in Figure 4).*

Rate Effects on Mean Tensile Strength

The remarkable hardening of the brittle response with the rate increase, discussed previously by Mastilovic et al. (2008) and Mastilovic (2010), is illustrated in Figure 4. The solid circle represents the mean strength obtained from 30 different statistical realizations at the five selected strain rates. The hollow circles depict one single realization at eight additional strain rates. The increase of the loading rate results in increase of the mean tensile strength, limited by the two horizontal asymptotes (σ_{m0} and σ_m^{th}) dependent on the system disorder (Mastilovic, 2010). The loading rate increase (corresponding to increasingly adiabatic deformation and damage) also results in the reduction of response stochasticity caused by the averaging effect of collective behavior of microcrack systems that smoothens the randomness at the macroscopic scale and by the diminishing flaw-sensitivity of brittle materials with the loading-rate increase (Mastilovic et al., 2008).

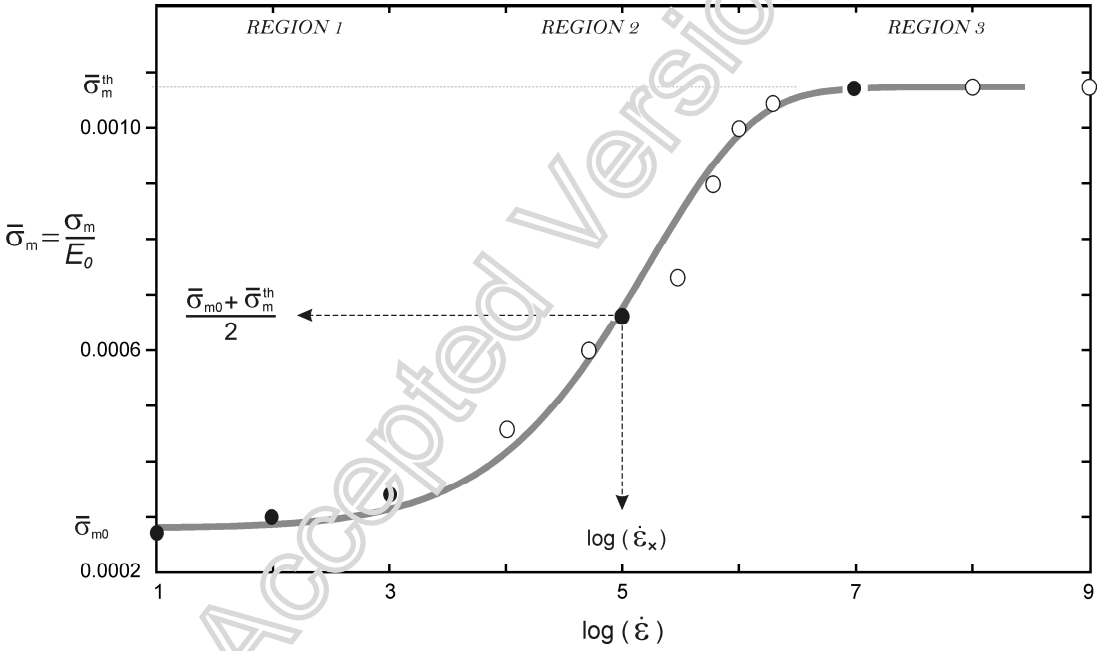

Figure 4. *Mean tensile strength vs. strain rate. Solid line represents a fit obtained by using Equation (3) with parameters: A=4.7, C=12, and* $\dot{\varepsilon}_\times = 1\times10^5\ s^{-1}$.

Based on the simulation results, the following expression

$$\sigma_m = \sigma_{m0} + S_m \left\{1 - \exp\left[-\left(\frac{\log(\dot{\varepsilon}) + A}{2\log(\dot{\varepsilon}_\times)}\right)^C\right]\right\} \tag{3}$$

is proposed to capture general features of the mean tensile strength dependence on the strain rate. A similar expression was subject to a limited discussion by Mastilovic (2010) with regards to the material disorder effects on the tensile strength, without going into details of the rate dependence. That is, the parameter $S_m = S_m(\alpha,\beta) = \sigma_m^{th} - \sigma_{m0}$ is a measure of hardening and A, C, and $\dot{\varepsilon}_\times$ are fitting parameters.

As indicated on Figure 4, the crossover strain rate $\dot{\varepsilon}_{\times}$ corresponds to $\sigma_m = (\sigma_m^{th} + \sigma_{m0})/2$. It should be noted that the theoretical strength, associated by Grady (1995) with the Hugeniot elastic limit obtained from shock compression experiments, is attained here by the virtual *tensile* experiments. The demonstrated disorder dependence of the hardening parameter S_m (Mastilovic, 2010) suggests that the degree of structural heterogeneity of brittle solid governs substantially the process of activation and nucleation of micro-defects.

The effect of fitting parameters on the character of the strength-rate curve is visualized in Figure 5. Roughly, the parameters A and $\dot{\varepsilon}_{\times}$ define the onset of the strength rapid increase, while C defines gradient of that increase.

It is obvious from Equation (3) that the quasi-static strength (σ_{m0}) is not truly a horizontal asymptote but the lower limit that is reached at $\log(\dot{\varepsilon}) = -A$. Furthermore, the solid curve in Figure 4 has a symmetric negative branch that has no physical meaning in the present context. Nonetheless, this should not be a serious application obstacle not only because it is easily algorithmically resolved but also since the negative branch increase remains practically insignificant deep into the quasi-static loading range (for example, for the data fit in Figure 4, until $\log(\dot{\varepsilon}) \approx -10$).

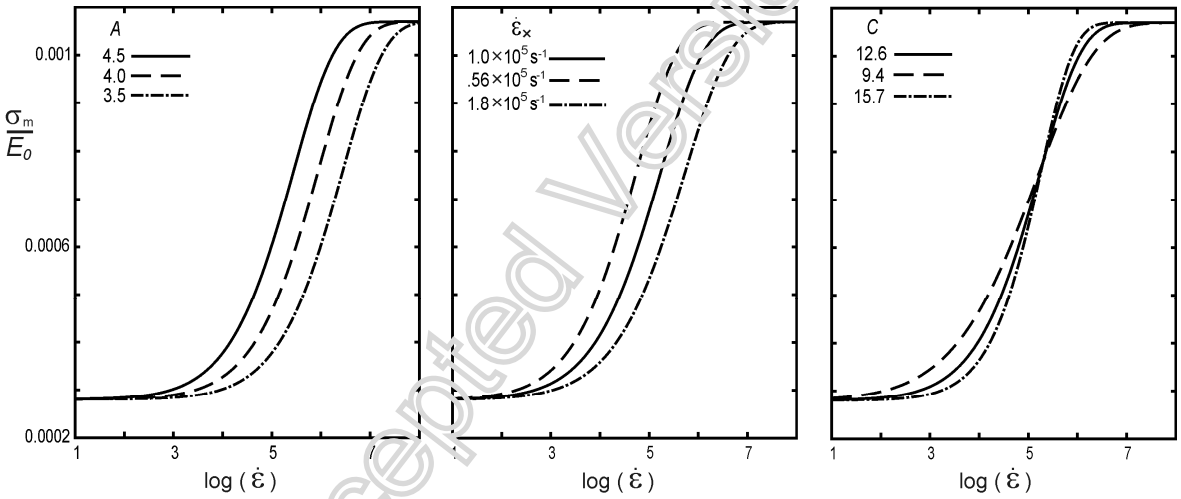

***Figure 5.** Effect of strength parameters on the shape of the strength-rate curve.*

In summary, at extreme loading powers (Region 3 in Figure 4), the upper-asymptote strength of brittle systems is achieved through effective suppression of the cooperative phenomena, which drive the rapid strength increase in the transitional range (Region 2). On the other hand, at the low-to-medium loading powers (Region 1), the sample strength seems to be determined to a large extent by the stochastic distribution of intrinsic defects and more sensitive to boundary conditions, since a few weak links (i.e., the microcracks thermally activated at the intrinsic defect locations) govern the catastrophic failure of the sample. The simplicity of Equation (3) is, thus, remarkable since it appears that experiments at only a couple of carefully selected strain rates (perhaps as little as three) would suffice to define with reasonable confidence the strength evolution within the entire strain rate range.

Time to Failure and Damage Dynamics

In the course of rapid energy input (the high loading power, Region 3), the kinetic energy of the sample exceeds its potential energy by a few orders of magnitude (Mastilovic et al., 2008) and the dominant mechanism of damage growth is the nucleation and activation of microcracks (Figure 1a) as already discussed. On the other hand, clustering of microcracks into microcrack clouds, and cooperative

phenomena on both microscopic and mesoscopic scales, that culminate in failure, are accompanied by a relative balance of potential and kinetic energies. For the rates resulting in brittle failure and the strength asymptotically approaching the lower strength (quasi-static) plateau, the potential energy exceeds the kinetic energy until the sample failure. The damage pattern just before the stress peak (see left-side snapshots in Figure 1) and corresponding damage energetics are particularly interesting points that are frequently neglected (Van Mier and Man, 2009). Hence, an emphasis of this investigation on the stress-peak and immediate post-peak behavior of the low fracture energy systems.

Typically, the stress-peak state of material is, for both the low and the extremely high loading rates, characterized by insignificant damage, which is followed by rapid increase of damage (localized in the former and uniformly distributed in the later case).

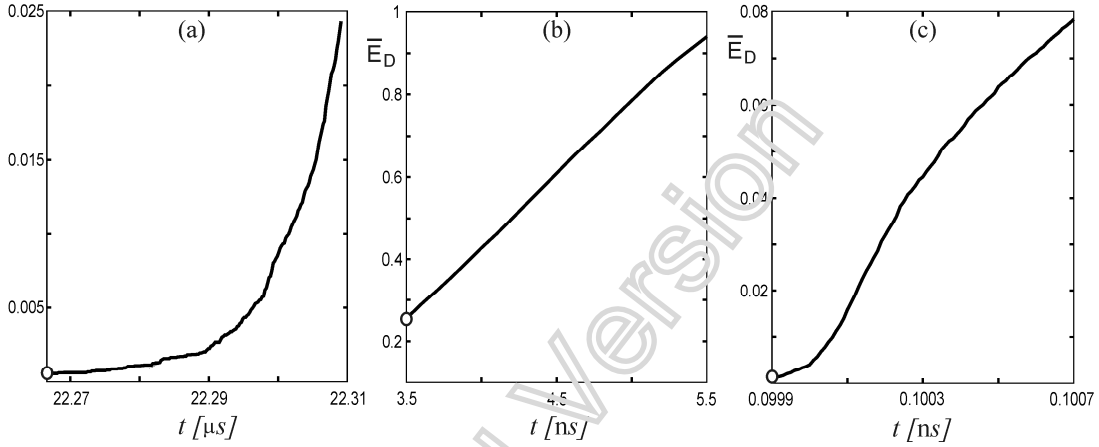

Figure 6. *Typical post-peak time histories of damage energy for three different loading rates: (a) 10 s^{-1}, (b) 3×10^5 s^{-1}, (c) 1×10^7 s^{-1}. The hollow circles mark the stress-peak values. The damage energy is normalized with the strain energy released upon the rupture of one single bond with average properties, $\bar{k}\,\bar{\lambda}_0^2\,\varepsilon_{cr}^2/2$.*

This is illustrated by Figures 6a and 6c that present typical damage energy evolution immediately following the stress-peak state for 10 s^{-1} and 1×10^7 s^{-1}, respectively. (Note that the hollow circle in each graph represents the stress-peak value.) As mentioned before, both of these loading rates are characterized by absence of substantial cooperative phenomena: (i) in the low-rate limit, corresponding to the quasi-static asymptote, the early developed dominant microcrack cluster (macrocrack) governs the response of the damaged material and (ii) in the high-rate limit corresponding to upper-strength plateau, the material response is characterized by the abrupt uniform microcrack nucleation. The development of the web of cooperating microcrack clouds (Figure 1c), accompanied by the strength surge (Region 2 in Figure 4), gradually evens out the difference in damage energy rates at the stress peak ($\dot{E}_{Dm}$) and immediately after ($\dot{E}_{Df}$) (Figure 6). The strain rate $\dot{\varepsilon}_{eq} = 3\times10^5\ s^{-1}$ is characterized by, practically, complete absence of the damage energy rate change in the peak neighborhood ($\dot{E}_{Df} \approx \dot{E}_{Dm}$, Figure 6b) and corresponds to the most ductile-like stress-strain curve (Mastilovic et al., 2008).

The rate-driven change of the damage energy rate during softening is summarized in the logarithmic plot in Figure 7; the hollow squares represent the mean of 30 statistical realizations while the solid circles mark results of one single realization at the given rates. Note that, due to the observed reduction of the data scatter with the increase of loading rate, any arbitrarily selected physical realizations at the high rates should represent reasonably well the mean value. The dashed line in Figure 7 represents the best fit of the simulation data:

$$\log\left(\frac{\dot{E}_{Df}}{\dot{E}_{Dm}}\right) = H_1\left\{\left(\log\dot{\varepsilon} - \log\dot{\varepsilon}_{eq}\right) - H_2\left[\exp\left(\frac{\log\dot{\varepsilon} - \log\dot{\varepsilon}_{eq}}{H_2}\right) - 1\right]\right\} \tag{4}$$

where H_1 and H_2 are fitting parameters and $\dot{\varepsilon}_{eq}$ is the strain rate corresponding to the stress-peak damage energy rate equilibrium ($\dot{E}_{Df} = \dot{E}_{Dm}$) that marks the minimum of the dashed curve in Figure 7.

It is obvious that the asymmetric data fit in Figure 7, defined by Equation (4), formally tends to infinity for both loading limits (the quasi-static and the "infinite"), but for different reason: $\lim_{\dot{\varepsilon}\to 0}\dot{E}_{Dm} = 0$ and $\lim_{\dot{\varepsilon}\to\infty}\dot{E}_{Df} = \infty$, respectively. In reality, the maximum possible strain rate in the material, ε_0 (Introduction), provides the finite limit for $\dot{E}_{Df}$, while the stress peak is by definition associated by non-zero $\dot{E}_{Dm}$ (albeit very small and temporal-resolution dependent for the low rate "limits").

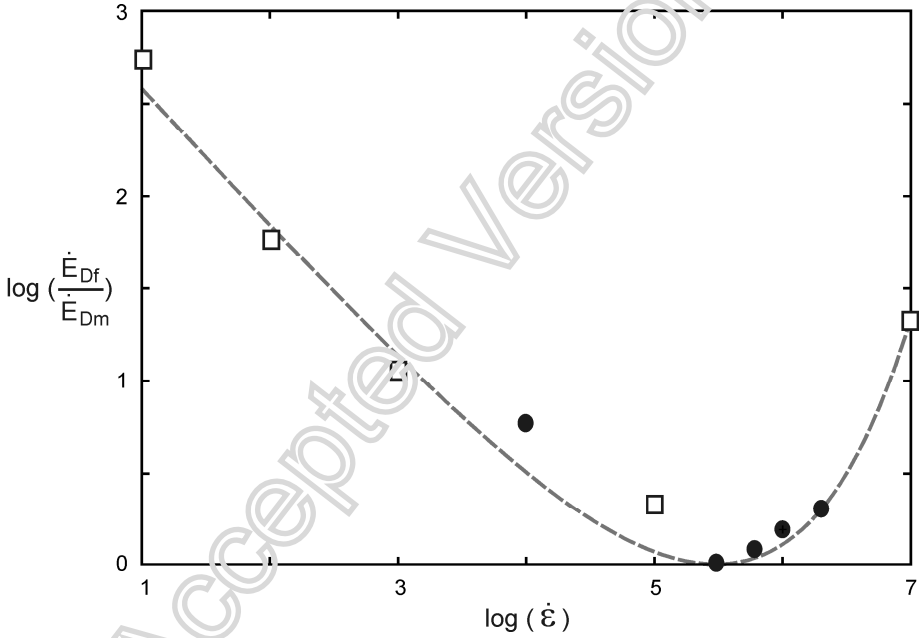

Figure 7. *Change of the ratio of damage energy rates in the post-peak and peak regions of stress-strain curve with the loading rate. Dashed line represents the fit obtained by using Equation (4) with fitting parameters H_1=-0.76, H_2=1.1, and* $\log\dot{\varepsilon}_{eq} = \log\left(3\times10^5\right) = 5.48$.

Figure 8 illustrates effect of the loading rate on the damage energy rate (the hollow squares) at the stress-peak and the corresponding time, t_m, at which it is reached (the solid circles). The stress-peak time is tentatively affiliated with time-to-failure in this investigation for two reasons: (1) the sample would fail at the stress-peak for the stress-controlled test, and (2) the prevalent opinion, matured over the last two decades, is that the softening is not an intrinsic material property (e.g., Krajcinovic, 1996; Van Mier and Man, 2009). Time to failure is a highly stochastic variable. All data points in Figure 8 represent mean values of 30 statistical realizations per strain rate.

The linearity of the rate dependence of the peak parameters

$$t_m\ \dot{\varepsilon} = Const. \tag{5}$$

$$\frac{\dot{E}_{Dm}}{\dot{\varepsilon}} = Const. \tag{6}$$

is evident from Figure 8. Equation (5) is identical to the empirical relationship between creep rate and time to rupture for the constant-stress quasi-static loading (Tetelman and McEvily Jr., 1967), and the strain-controlled brittle creep fracture by Kachanov (1986). It also bears similarity with the time to failure derived by Mishnaevsky Jr. (1998) by combining the main ideas of continuum damage mechanics and statistical and kinetic theories of strength.

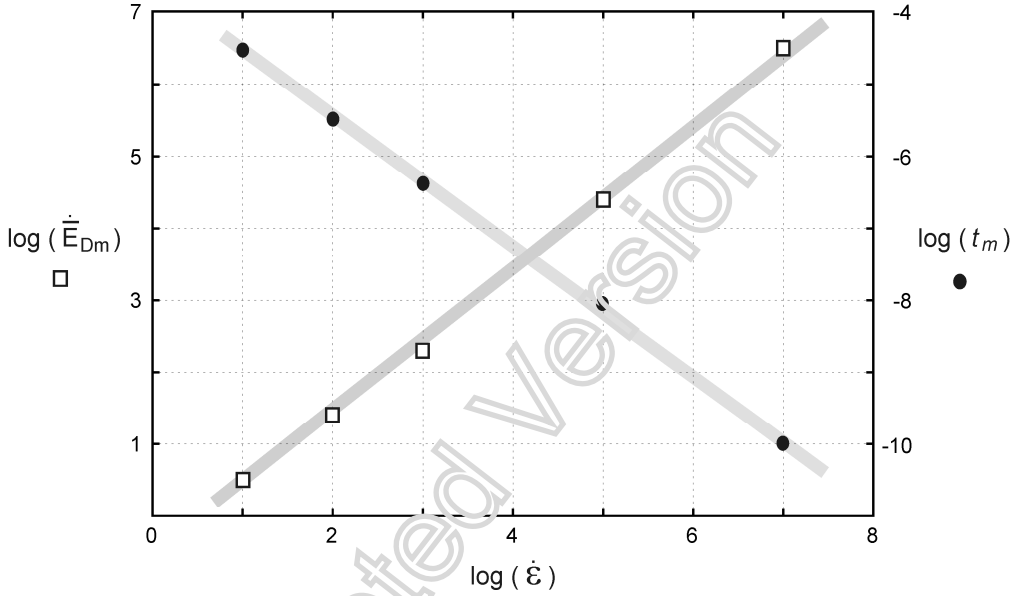

Figure 8. *Change of the mean stress-peak parameters with the loading rate; hollow squares represent the mean damage energy rate and solid circles the mean stress-peak time.*

Furthermore, it can be observed that, for the discrete model used in this investigation, the constants in Equations (5) and (6) are related to the failure criterion at the microscopic scale:

$$t_m \, \dot{\varepsilon} \propto \varepsilon_{cr}^{-1} \tag{7}$$

$$\frac{\dot{E}_{Dm}}{\dot{\varepsilon}} \propto \varepsilon_{cr}^{-1/6} \tag{8}$$

It is noteworthy that Equations (7) and (8) relate the macroscopic response parameters at the stress peak (t_m, $\dot{E}_{Dm}$) to the microscopic failure criterion (ε_{cr}) for the dynamic loading within the wide range of the strain rates that encompasses variety of damage mechanisms.

Size Sensitivity of Simulation Results

The size sensitivity of the dynamic lattice model used in this study is investigated originally by Mastilovic and Krajcinovic (1999). The focus of that early work was on the tensile strength, consequently, the mesh objectivity analysis was limited to sample-size strength sensitivity. A notable extension of the present study, in addition to repeated simulations for different physical realizations of microstructural

statistics, is the analysis of the damage energy density rate and time to failure; accordingly, it is necessary to revisit the mesh sensitivity analysis for the entire loading rate range.

The mesh sensitivity of the simulation results obtained by using 192×227 lattice (43,584 continuum particles) is explored by comparison with those obtained with 384×455 (174,720), 576×681 (393,256), and 768×909 (698,112) lattices, which correspond to the size increase of 300%, 800% and 1500%, respectively. Table 1 presents the difference in tensile strength, time to failure, and damage energy density rates for one single realization at the four selected strain rates in the range [1×10^3 s^{-1}, 1×10^7 s^{-1}]. For example, $Dif\,(\sigma_m) = 100\times(\sigma_{mN}-\sigma_{mS})/\sigma_{mS}$, is a percentage difference between tensile strength obtained for the original lattice, 192×227 (σ_{mS}), and one of the other three verification lattices (σ_{mN}).

Table 1. Difference [%] between results of one single realization of 192×227 vs. 384×455 lattices, 192×227 vs. 576×681 lattices, and 192×227 vs. 768×909 lattices respectively; and between mean values of 15 realizations of 192×227 vs. 384×455 lattices at 100 s^{-1}.

$\dot{\varepsilon}\,[s^{-1}]$	$Dif\,(\sigma_m)$	$Dif\,(t_m)$	$Dif\,(\dot{E}_{Df}/\Omega)$	$Dif\,(\dot{E}_{Df}/\Omega)$
	192×227 vs. 384×455, 192×227 vs. 576×681, 192×227 vs. 768×909			
1×10^7	0.13, 0.27, 0.32	-0.030, 0.00, 0.010	-1.39, 3.99, 4.42	0.98, 2.93, 3.42
1×10^5	-0.41, -0.70, -0.45	-0.45, -0.23, -0.23	-3.38, -2.03, -0.68	-0.92, 0.00, 0.62
1×10^4	-1.43, -2.87, -2.22	-2.01, -3.02, -2.35	1.83, 4.59, -3.67	-3.77, -1.89, -0.94
1×10^3	-1.89, -9.05, -8.91	-0.54, -7.93, -7.73	10.0, 2.58, -3.48	14.6, 3.20, -2.46
100	-4.5	-4.0	1.2	-4.2

The results indicate negligible size sensitivity of the tensile strength and time to failure for the two highest rates. The strain energy density release rates are more sensitive, but still with a relatively small difference. The decrease in loading rate results in more pronounced size effect, but generally within acceptable limits as illustrated graphically for $|Dif\,(\sigma_m)|$ on Figure 9.

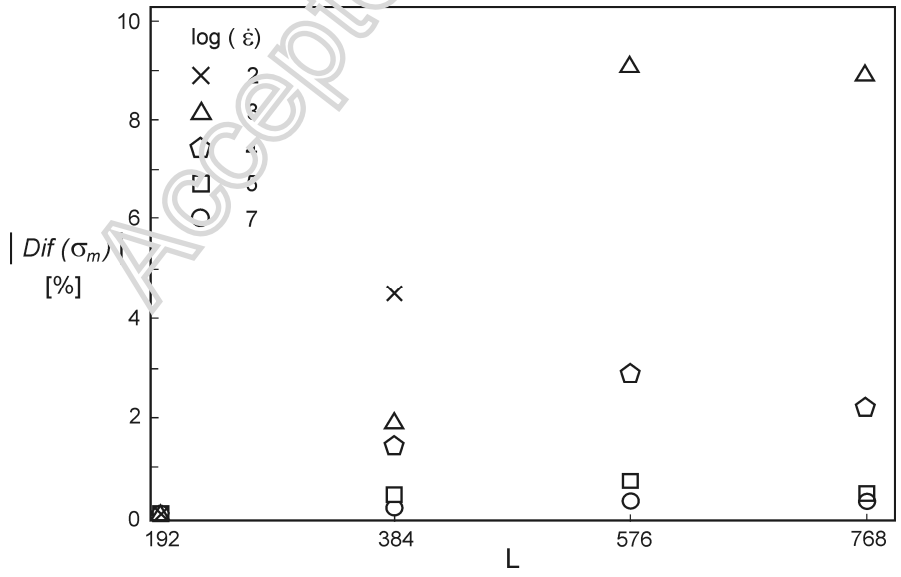

Figure 9. *Illustration of size effect on $|Dif\,(\sigma_m)|$ for various strain rates.*

It is noteworthy that while the damage energy density values at any particular time can be notably different for the four lattice sizes, the damage energy density rates corresponding to stress-peak and ultimate failure are relatively insensitive to the lattice size.

Figure 9 illustrates observed reduction of size effect on $|Dif(\sigma_m)|$ with increase of loading rate, which is consistent with general trend of the reduction of stochasticity with the loading rate increase (Mastilovic et al., 2008). It should be noted that Hansen et al. (1989) obtained for the static case the lattice size scaling of the peak force in the form $F_m \propto L^{\chi}$ and determined the exponent χ to be 3/4. Although this peak force is directly related to the tensile strength, σ_m, no such regularity is observed in the present work. It is important to note, on that account, not only a number of differences between the two brittle lattices but also that the present size inquiry is limited to one physical realization, while Hansen et al. (1989) obtained their results by averaging over a large number of samples, which would be prohibitively time consuming in the present case. Since such thorough size-effect analysis is beyond the scope of the present investigation, the statistical approach is not used, which makes the comparison of results iffy.

Nonetheless, since the results suggest that the loading rate reduction leads to increase of dependency upon the particular statistical realization, the comparison at 100 s^{-1} is performed on a randomly selected subset of 15 statistical realizations. Consequently, the last row of Table 1 presents the differences in mean values at 100 s^{-1}, while a selection of two corresponding histograms is given by Figure 10 (for computation economy, the comparison is performed only with 384×455 lattice). Figure 10 demonstrates that at the low strain rate results become increasingly both sample-size and realization dependent, especially the damage energy density rates. Furthermore, it is observed that while the change in lattice size from 192×227 to 384×455, at 100 s^{-1}, results in a relatively small difference in the mean tensile strength (-4.5%), the difference in the strength scatter is more pronounced: the standard deviation is reduced by 15%.

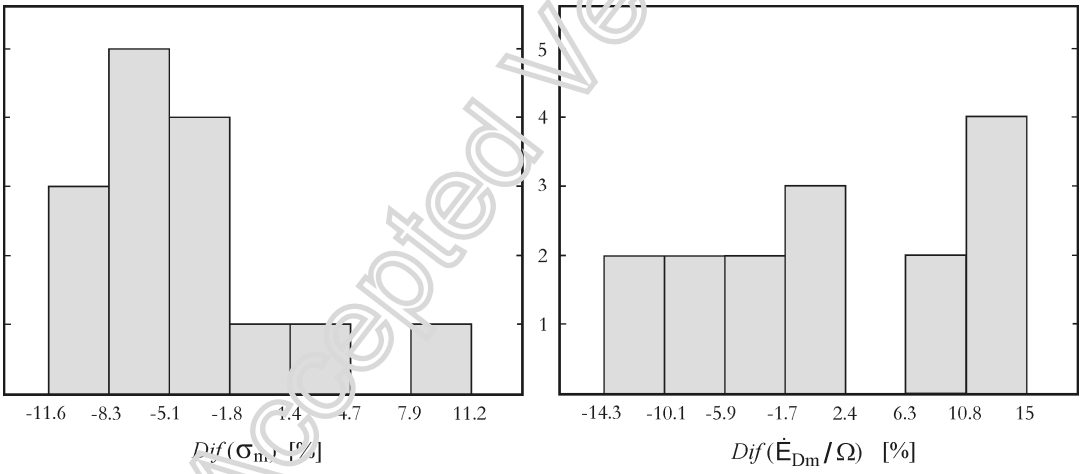

Figure 10. *Histograms of differences in the maximum stress (tensile strength) and the corresponding damage energy density rate between192×227 and 384×455 lattices at 100 s^{-1}.*

In summary, the results of virtual experiments at the moderate rates (Region 1) presented herein could benefit somewhat by increase of both sample size and "ensemble" size. On the other hand, since the lattice size in the present model corresponds to the spatial averaging region, it must be, as any representative volume element in general, "small enough to avoid smoothening of high gradients but large enough to represent an average of the microprocesses" (Lemaitre, 1992). Altogether, keeping in mind the relatively modest size sensitivity of results and the primarily qualitative nature of the present study it seems justified to assert that the corresponding observations and conclusions are not affected by the lattice size and that the 192×227 lattice is fairly representative.

SUMMARY

This study elucidates some universal trends that contribute to understanding of basic principles governing high-rate mesomechanics of heterogeneous low-fracture-energy solids. An expression proposed to model the mean tensile strength dependence on the strain rate for the entire strain rate range is discussed. Although the fundamental arguments to support the form of this expression could not be provided at present, it appears simple and robust enough to capture reasonably well the entire rate-driven strength evolution with only a few experiments.

The damage dynamics is investigated based on change in the damage energy rate accompanying damage evolution in the stress-peak neighborhood. It is noticed that the medium of the transitional range rates (Region 2), $\dot{\varepsilon}_{eq} = 3\times10^5\ s^{-1}$, is characterized by the absence of change of the damage energy rate in the peak neighborhood ($\dot{E}_{Df} \approx \dot{E}_{Dm}$) and corresponds to the most ductile-like stress-strain curve.

The linearity of the rate dependence of the stress-peak macroscopic response parameters is outlined. The simulation results offer connection between the macroscopic response parameters at the stress peak (t_m, $\dot{E}_{Dm}$) and the microscopic failure criterion (ε_{cr}) for the dynamic loading within the wide range of the strain rates that encompasses variety of damage mechanisms.

ACKNOWLEDGMENT

The author gratefully acknowledges the financial support by the Ministry of Science and Technology of the Republic of Serbia.

REFERENCES

Bhattacharya, K., Ortiz, M., Ravichandran, G., 1998. Energy-based model of compressive splitting in heterogeneous brittle solids. J. Mech. Phys. Solids 46 (10), 2171-2181.

Cundal, P.A., Strack, O, D., 1979. A discrete numerical model for granular assemblies. Geotecnique 29, 45-65.

Curtin, W.A., Scher, H., 1990. Brittle fracture in disordered materials: a spring network model. J. Mater. Res. 5, 535-553.

Drugan, W.J., 2001. Dynamic fragmentation of Brittle materials: analytical mechanics-based models. J. Mech. Phys. Solids 49, 1181-1208.

Espinosa, H.D., Zavattieri, P.D., 2003. A grain level model for the study of failure initiation and evolution in polycrystalline brittle materials. Part I: Theory and numerical implementation. Mech. Mater. 35, 333-364.

Field, J.E., Walley, S.M., Proud, W.G., Goldrein, H.T., Siviour, C.R., 2004. Review of experimental techniques for high rate deformation and shock Studies. Int. J. Impact Eng. 30, 725-775.

Grady, D.E., 1995. Dynamic Properties of Ceramic Materials. SAND 94-3266, Sandia National Laboratories, Albuquerque.

Hansen A., Roux S., Herrmann H.J. (1989). Rupture of central-force lattices. *J. Phys. France* **50**: 733-744.

Holian, B.L., Grady, D.E., 1988. Fragmentation by Molecular Dynamics: The Microscopic "Big Bang." Phys. Rev. Lett. 60 (14), 1355-1358.

Jagota, A., Bennison, S.J., 1994. Spring-Network and Finite-Element Models for Elasticity and Fracture, in: Bardhan, K.K., Chakrabarti, B.K., Hansen, A. (Eds.), Proceedings of a workshop on breakdown and non-linearity in soft condensed matter, Springer-Verlag Lecture Notes in Physics, Berlin, pp. 186-201.

Jirasek, M., Bazant, Z. P., 1995. Macroscopic fracture characteristics of random particle systems. Int. J. Fract. 69, 201-228.

Kachanov L.M., 1986. Introduction to Continuum Damage Mechanics. Martinus Nijhoff Publishers, Dordrecht, The Netherlands

Krajcinovic, D., 1996. Damage Mechanics. North-Holland, Amsterdam, The Netherlands.

Kuksenko, V.S., Ryskin, V.S., Betekhtin, V.I., Slutsker, A.I., 1975. Nucleation of submicroscopic cracks in stressed solids. Int. J. Fract. 11 (5), 829-840.

Lawn, B. 1993. Fracture of Brittle Solids, second ed. Cambridge University Press, Cambridge.

Lemaitre, J. 1992. A Course on Damage Mechanics. Springer-Verlag, Berlin.

Liu, J.X., Deng, S.C., Liang, N.G., 2008. Comparison of the quasi-static method and the dynamics method for simulating fracture process in concrete. Comput. Mech. 41, 647-660.

Mastilovic, S., 2008. A Note on Short-Time Response of Two-Dimensional Lattices During Dynamic Loading. Int. J. Damage Mech. 17, 357-361.

Mastilovic, S., 2010. Some Observations Regarding Stochasticity of Dynamic Response of 2D Disordered Brittle Lattices. Int. J. Damage Mech. doi: 10.1177/1056789509359674.

Mastilovic, S., Krajcinovic D., 1999. Statistical Models of Brittle Deformation, Part Two: Computer Simulations. Int. J. Plast. 15, 427-456.

Mastilovic, S., Rinaldi, A., Krajcinovic, D., 2008. Ordering effect of kinetic energy on dynamic deformation of brittle solids. Mech. Mater. 40 (4-5), 407-417.

Mishnaevsky Jr., L., 1998. Damage and Fracture of Heterogeneous Materials. A.A. Balkema, Rotterdam, The Netherlands

Monette, L., Anderson, M. P., 1994. Elastic and fracture properties of the two-dimensional triangular and square lattices. Model. Simul. Mater. Sci. Eng. **2**: 53-66.

Ostoja-Starzewski, M., 2002. Lattice models in micromechanics. Appl. Mech. Rev. 55 (1), 35-60.

Raiser, G., Clifton, R. J., Ortiz, M., 1990. A soft-recovery plate impact experiment for studying microcracking in ceramics. Mech. Mater. 10, 43-58.

Rinaldi, A., 2009. Rational Damage Model of 2D Disordered Brittle Lattices Under Uniaxial Loadings. Int. J. Damage Mech. 18, 233-257.

Rinaldi, A., Krajcinovic, D., Peralta, P., Lai, Q., 2008. Lattice models of polycrystalline microstructures: A quantitative approach. Mech. Mater. 40, 17-36.

Qi, C., Wang, M, Qian, Q., 2009. Strain-rate effects on the strength and fragmentation size of rocks, Int. J. Impact Eng. 36, 1355-1364.

Sarva, S., Nemat-Nasser, S., 2001. Dynamic compressive strength of silicon carbide under uniaxial compression. Materials Science and Engineering, **A317**: 140-144.

Tetelman, A.S., McEvily Jr., A.J., 1967. Fracture of Structural Materials. John Wiley & Sons, New York.

Van Mier, J.G.M., Man, H., 2009. Some Notes on Microcracking, Softening, Localization, and Size Effect. Int. J. Damage Mech., 18 (3), 283-309.

Wang, H., Ramesh, K.T., 2004. Dynamic strength and fragmentation of hot-pressed silicon carbide under uniaxial compression. Acta Mater. 52, 355-367.

Weiner, J. H., 2002. Statistical Mechanics of Elasticity. 2nd Edition. John Wiley & Sons, New York.

Zallen, R. (1983) The Physics of Amorphous Solids, John Wiley & Sons, New York, New York

Zhou, F., Molinari, J.F., 2004. Stochastic fracture of ceramics under dynamic tensile loading. Int. J. Solids Struct. 41, 6573-6596.